Construction and Characterization of a Biomimetic Robotic Eye Model with Three Degrees of Rotational Freedom: A Testbed for Neural Control of Eye Movements

Miguel Ruiz Callé Lucas

miguelruizlucas@gmail.com

Instituto Superior Técnico, Universidade de Lisboa, Portugal

October 2017

Abstract

How our brain is able to successfully control our movements is not yet fully understood. Even apparently simple tasks like recognizing and grabbing a pen from the table are still very difficult to achieve with current robots. This is not only because the robot's anatomy differs, but also because we still don't know the neural mechanisms that select the observed consistent muscle activations from infinitely many alternatives.

In this paper, we build and analyse a robotized eye that has some essential similarities to the real 3D human eye anatomy. The goal is to control this model eye in such a way that its movements resemble real human eye movements, and to get a better understanding of the underlying control principles of these movements. With it, we intend to approximate future robotic control to the human's nervous system, and also have a better comprehension of how the brain controls movement, and why it follows certain rules.

The preliminary experiments with our robotic eye provide some answers on how the neural constraints on eye orientation, described by Donders' and Listing's laws, may relate to its mechanics and dynamics. With this, we were able to determine the third degree of freedom (roll) trajectories with respect to Listing's Plane. Furthermore, we characterized the dynamics of our newly built system quantitatively, so that we may predict control signals that resemble the real brain commands.

Keywords: human eye anatomy, robotic eye, Donders' law, Listing's law, brain commands

1. Introduction

The Human body is a seemingly flawless machine. Despite the complexity of the human motor control system, a healthy subject seems to execute mechanical tasks nearly perfectly, with a large degree of reproducibility, throughout its lifespan. Because the number of degrees of freedom typically exceeds, by far, the required number of controllable degrees of freedom for the particular motor task, there are infinitely many possibilities for the brain to control its muscles. This is known as the 'degrees-of-freedom problem' (1), which is mathematically ill-posed.

A good illustration of the redundancy problem is the human eye. When designing a pair of eyes for a robot, engineers typically account for two degrees of freedom for each eye, i.e., horizontal (yaw) and vertical (pitch) rotations that specify the gaze direction. This will guarantee that the robot's eye can look anywhere within the visual field. In reality, however, the human eye has three movement degrees of freedom (yaw, pitch and roll), and it is controlled by six extra-ocular muscles, that can be functionally grouped into three antagonistic muscle-pairs (2). As these three pairs are approximately orthogonally organized with respect to each other, they span a 3D Cartesian space. Thus, each pair is in charge of one degree of freedom. However, because the main activation directions of the two vertical-torsional eye-muscle pairs are not arranged along the purely vertical and torsional directions, each vertical eye orientation typically depends on the joint activation of both pairs of torsional-vertical muscles. In this work, we will design a biologically inspired robotized eye with three degrees of freedom. We will characterized this prototype and

experiment on it in order to find out why the eye movements obey certain rules. The goal is to approximate future robot design to the human anatomy.

2. Background

2.1. Eye mechanics

The eyeball or globe is approximately spherical (2) and rests within the orbita. It is encircled by six extraocular muscles which, apart from being accountable for exceptionally fast and precise eye movements, they firmly secure the eyeball inside the orbita. The geometrical arrangement of the six extra-ocular muscles is approximately parallel to the three planes of the semi-circular canals of the vestibular system. The muscles, displayed in Figure 2.1, are named (3): Superior Rectus (SR), responsible for upward and intorsional movement; Inferior Rectus (IR), responsible for downward and extorsional movement; Superior Oblique (SO), responsible for downward and intorsional movement; Inferior Oblique (IO), responsible for upward and extorsional movement; Medial Rectus (MR), which is responsible for horizontal inward movement; Lateral Rectus (LR), responsible for horizontal outward movement.

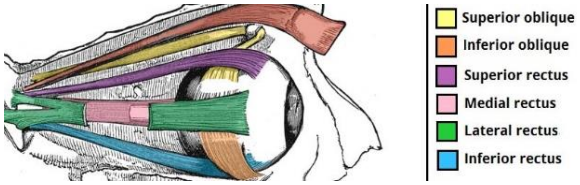

Figure 2.1: Extraocular muscles of the right eye *(4)*

The elastic properties of these muscles are almost identical, with the major differences being their insertion points and trajectories on the globe. Note that the Superior Oblique (in Yellow) before inserting on the eye, passes through a small cavity called Trochlea. Furthermore, all muscles except for the Inferior Oblique (Orange) arise from a tendinous band surrounding the optic nerve behind the eye, called the annulus of Zinn. In contrast, the IO muscle originates from the orbital plate of the maxilla (occulted by the eye in Figure 2.1). The distinctive geometrical paths of the IO and SO muscles cause their major pulling actions to be an intorsional (SO) and extorsional (IO) rotation around the visual axis.

Figure 2.2 defines the right-handed 3D Cartesian coordinate system that will be used in this paper, and the pulling directions of the extraocular muscles of the right eye in this reference frame. Note that (+x) is the forward direction, and a positive rotation along this axis will correspond to a clockwise torsional movement of the eye. Similarly, the +y axis is along the inter-ocular direction, and a positive rotation causes a downward rotation. Finally, the +z axis is oriented vertically, and positive rotation is leftward (action of the MR for the right eye). Note that MR-LR, SO-IO, and SR-IR have their pulling actions in opposite directions (2). They therefore constitute an antagonistic pair of muscles. For a given direction within the three muscle plains, the muscle being contracted is called the agonist. The muscle that would make the eye rotate in the opposite direction is then the antagonist. For instance, if one is to make a pure inward movement with the right eye, the MR muscle would be contracted (agonist), while the LR would have to relax (antagonist).

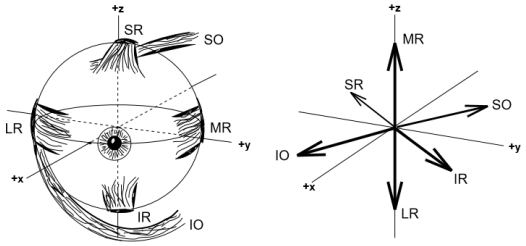

Figure 2.2: Axis notation and frontal view of the right eye where (+x) marks the primary direction. Note that the eye is rotated 15° towards the nose *(5)*

2.2. Eye orientation rules

The orientation of the eye can be predicted by assuming that the trajectory from the primary direction to the intended gaze point follows a geodesic (shortest path between two points on the surface of a sphere). The primary direction is the normal vector to Listing's plane (see below). Moreover, it was found that these movements obey certain rules even during the trajectory, which can be well described as single-axis rotations of a fixed body. To get a better understanding of these concepts, we must first explain some basic eye laws, which were already formulated in the 19th century by Von Helmholtz, based on careful observations and experiments performed by Donders and Listing.

Donders' Law

Donders' law states that the torsional component of the eye's orientation (x) only depends on the pointing direction of the visual axis (y,z), no matter how the eye arrived at that gaze direction. For example, suppose we first look forward and then look up, and as an alternative, we first look to the side, and then reorient the eyes until we reach our desired upward gaze position. Donders' law then

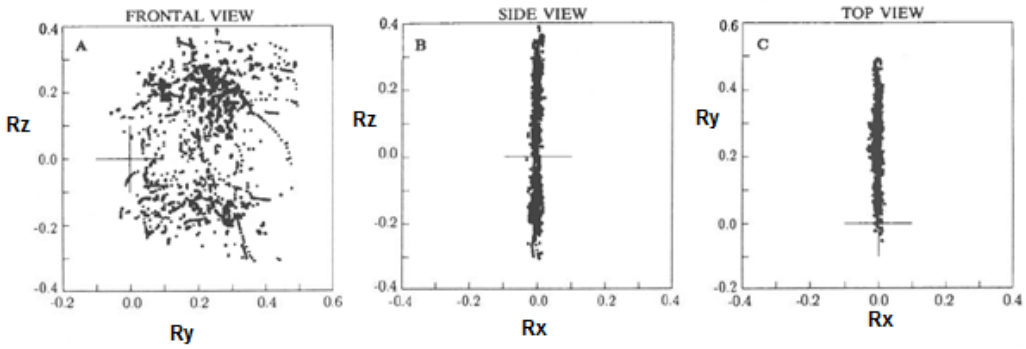

Figure 2.3: Experimental verification of Listing's law. Measures are in half-radians where 0.1 half-radian corresponds to about 10 degrees. Note that the components correspond to the coordinates of the rotation vectors: r_z (rotation about z-axis); r_y (rotation about the y-axis); r_x (rotation about x-axis). The centre of the monkey's oculomotor range is about 30 degrees below the primary position (which is at zero) *(6)*

tells us that the 3D angular orientation of the eye will be the same for both situations (7). Donders' law is thus formalized (in quaternion terms) as:

$$q_x = f(q_y, q_z) \;\; Donders' \; Law \qquad (2\text{-}1)$$

with $f()$ a particular function, defining the 2D surface within the 3D space of orientations, and (q_x, q_y, q_z) the three Cartesian coordinates of the associated eye-orientation quaternion (see below, for more details on this algebraic representation).

Listing's Law

Listing's law may be interpreted as a further specification of Donders' law. It is applicable for the eye when looking at infinity (i.e. >1.5 m away) and with the head not moving and upright (8). In the appropriate frame of reference (when +x is the primary direction), so-called Listing's coordinate system, it simply says that:

$$q_x = 0 \quad Listing's \; Law \qquad (2\text{-}2)$$

Listing therefore proposed that all admissible eye orientations lie in a plane (Listing's Plane), for which the torsional component is zero.

Listing's Law has later been verified through numerous psychophysical experiments with monkeys and humans. The monkey/human would sit in a chair with the head restrained, and saccadic and smooth-pursuit eye movements would be recorded at a 1000 Hz sampling rate, while the subject was looking around the laboratory room (9).

Figure 2.3 shows the results of one of those experiments with a monkey. Looking at the frontal view of the eye-position data (the rotation-vector YZ plane, see also below, for conventions), we note that the monkey looked all across its oculomotor range (between about [0 to +50] degrees vertically, and [-40 to +40] degrees horizontally). What is interesting is that the side view and the top view show virtually zero torsion, meaning that all the recorded points lay in a well-defined plane $R_x = 0$.

2.3. Saccades Properties

During Saccadic movements, the human vision becomes blurred. For this reason, the duration must be at its minimum. At peak velocities exceeding $500\ deg/s$, the eye movement is among the fastest that the human motor system can produce (in monkeys, peak velocities reach even up to about $1200\ deg/s$ (9)). The human eye can only see sharply within $1-2°$ around the central fixation point. This means that we couldn´t identify an object or a person just by starring at them since the object wouldn´t fit within the foveal visual frame. What actually happens when we visually explore an object, is that we constantly make saccades (see Figure 2.4).

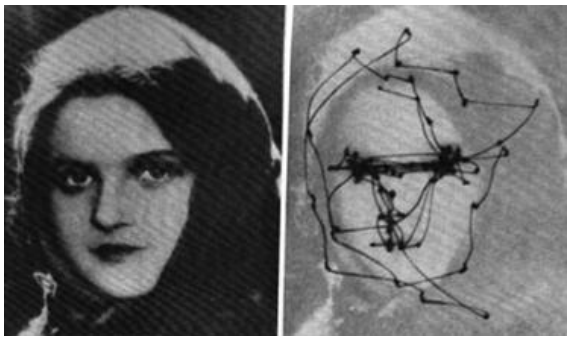

Figure 2.4: Early recording of saccadic eye movements. Note that saccades land on conspicuous high-contrast locations in the picture that provide most information about the picture's content: the mouth, nose and eyes *(10)*

The short movement durations of saccades ($50 - 100\,ms$) are somewhat surprising, considering the fact that the oculomotor plant (eye muscles, globe and surrounding fatty tissues) form a viscous, overdamped system with a long time constant of about $200\,ms$ (11). This low-pass time constant greatly exceeds the typical saccade duration. The Laplace transformation of the plant transfer function has been described by a second order overdamped system, with one real-valued zero, and two real-valued negative poles (11):

$$H(s) = C\frac{(sT_Z + 1)}{(sT_1 + 1)(sT_2 + 1)} \qquad (2\text{-}3)$$

where $T_2 = 20$, $T_Z = 70$ and $T_1 = 200\,ms$ and C a scaling factor that depends on the three time constants. To overcome the slow mechanics, the brain creates a pulse-slide-step input signal. This signal has been experimentally verified by neural recordings in the abducens nucleus (the motor neurons that innervate the LR muscle) of the monkey.

Figure 2.5 shows the response of a single abducens neuron PSTH (peri-saccadic time histogram) for 11 identical saccadic eye movements. Note the high reproducibility of the saccadic eye movements, and the extremely short duration (about $50\,ms$), which, indeed, make a good approximation of a step output. The pulse-slide-step input signal of the motor neurons (all abducens neurons fire in synchrony for this saccade) makes the eye travel faster, by overcoming the viscous forces without compromising speed and accuracy.

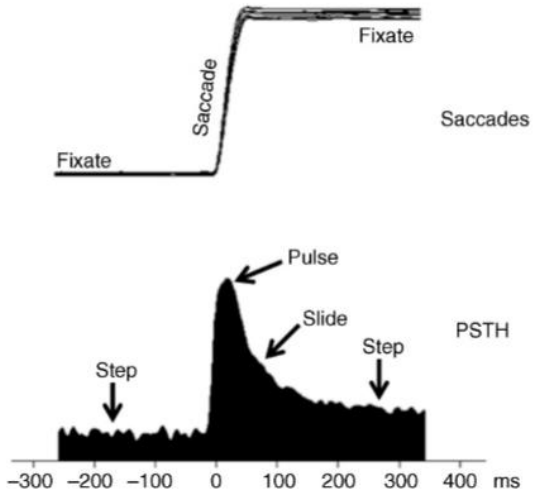

Figure 2.5: Recording of a oculomotor neuron muscle in macaque monkey for 11 rightward saccades *(11)*

2.4. Neural control of saccadic eye movements

The nonlinear characteristic of the saccadic system is usually attributed to a nonlinear (saturating) input-output property of the pulse generator (through burst cells) in the brainstem (see Figure 2.5, where the pulse is shown). These burst cells are thought to be driven by a dynamic motor error signal (the difference between the desired goal for the eye and the current eye displacement) and their output represents the desired velocity of the eye. The step signal in the motor neuron pulse-step (Figure *2.5*) is obtained by neural integration of this velocity signal. The figure below shows a simplified version of the model proposed by David A. Robinson (12) that explains how the system is driven by internal position feedback from the integrator to reach its goal (the desired orientation of the eye).

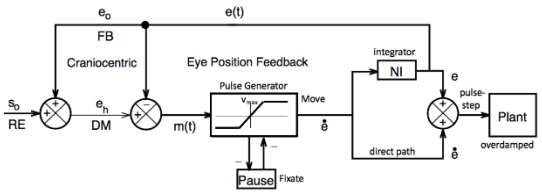

Figure 2.6: The Robinson model for saccadic eye movements *(12)*

In Figure 2.6, a target on the retina at s_0 is first transformed into a head-centred desired eye position e_h, by adding the initial position of the eye e_0. The desired position is continuously compared with the actual eye position $e(t)$, and the motor error $m(t)$, drives the nonlinear (saturating) pulse generator. The latter has a high gain and is under inhibitory control from pause cells. The pulse generator can fire only when the pause cells are stopped by a brief internal trigger signal. Once the pulse is generated to move the eye, it in turn inhibits the pause cells. The pulse output is a velocity signal that is integrated to current position by the neural integrator. Together, the (scaled) pulse and the integrated step form the pulse-step drive of the motor neurons to control the overdamped plant. The internal feedback guarantees that the saccade ends on the desired target.

2.5. Quaternions and Rotation Vectors

Quaternions are 4D complex algebraic entities, which turn out to be very useful to describe consecutive rotations of a body in a 3D environment. In general, a quaternion q is defined by:

$$q = (\, q_0, \vec{Q}.\vec{I}\,) = (q_0, q_1 i + q_2 j + q_3 k) \qquad (2\text{-}4)$$

where q_0 is a scalar and $\vec{Q}$ is a vector. $\vec{I} = [i, j, k]$ is a vector which components are complex numbers corresponding to the cardinal axes of the coordinate system (x, y, z) which follow the following rules: $i^2 = j^2 = k^2 = -1$, $ijk = -1$, $ij = k$, $ki = j$, $jk = i$. Without any loss of generality, we can normalize the quaternion $(length = 1)$, after which we can parametrize its four components as follows:

$$q_0 = cos\frac{\alpha}{2} \quad \text{and} \quad \vec{Q} = sin\frac{\alpha}{2}\hat{n} \qquad (2\text{-}5)$$

Note that α is the absolute angle of rotation in radians and $\hat{n}$ is the unitary vector of the axis of rotation ($\|\hat{n}\| = 1$).

The multiplication of two quaternions results in a new quaternion, but it is noncommutativity ($qp \neq pq$). It follows from the definition above, that the product of the quaternions $q = q_0 + \vec{Q}$ and $p = p_0 + \vec{P}$ is given by:

$$qp = (p_0 q_0 - \vec{P} \cdot \vec{Q}) + (p_0 \vec{Q} + q_0 \vec{P} + \vec{Q} \times \vec{P}) \qquad (2\text{-}6)$$

There is alternative parameterization of 3D rotations that is described by only three numbers, instead of four, and has been denominated in the oculomotor literature as the rotation vector. Provided by the Euler-Rodrigues coordinates, the rotation vector becomes quite useful during saccades in Listing's plane, since it can be mathematically shown that these follow straight lines in 3D rotation-vector space when viewed as fixed-axis rotations. The rotation vector r and its inverse r^{-1} are defined by (6):

$$r \equiv \frac{Q}{q_0} = \tan\left(\frac{\alpha}{2}\right)\hat{n} \quad \text{and} \quad r^{-1} = -r \qquad (2\text{-}7)$$

Making use of quaternion multiplication (equation (2-7)), it then follows that the combined result of rotation r_1 followed by a second rotation r_2 is given by (note the order in which the multiplication is written):

$$r_2 \circ r_1 = \frac{r_1 + r_2 + r_2 \times r_1}{1 - r_1 \cdot r_2} \qquad (2\text{-}8)$$

2.6. Describing Listing's Law and Saccades by Rotation Vectors

In this paper report, eye orientations (also called: eye positions), are represented using both Euler angle and rotation-vector notation, in which the Cartesian coordinates are initially taken as world-fixed. Later, when Listing's plane has been determined, the head-fixed reference frame will be in Listing's coordinates (also known as the primary reference frame) in which the origin $r_P = 0$ is called the eye's primary position. At the start of an experiment, the actual primary position is not yet known, and the origin is arbitrarily taken as the straight-ahead direction in the laboratory frame of reference, which corresponds approximately with the centre of the oculomotor range: $r_C = (r_x, r_y, r_z) = 0$.

Any orientation of the eye, say $r = r_A$, is now to be understood as a (virtual) rotation from the origin of the reference frame to the current orientation. Indeed, applying equation (2-8): $r_A = r_A \circ r_C$. Note that this description doesn't say anything about the actual trajectory that the eye took to reach that orientation.

After having recorded many different eye orientations across the oculomotor range, the joint set of eye positions will be distributed in 3D rotation-vector space. According to Listing's law, however, the 3D cloud of eye positions will be confined to a plane, called Listing's plane. In the laboratory reference frame this plane could in principle take any orientation in 3D space, and would in general be described by:

$$ar_X + br_y + cr_z = 0 \qquad (2\text{-}9)$$

with (a, b, c) the plane's normal vector and $a^2 + b^2 + c^2 = 1$. For monkeys and humans, it is typically found that $b = 0$, so that the plane seems rotated in the Lab's xz-projection.

3. Prototype

3.1. Mechanical Components

The idea of the core of the prototype came from a human shoulder joint and demonstrated with Lego® joints. The goal was to use a ball joint that could rotate freely and two simple pieces of Lego® proved that the model could work. A semi sphere would be attached to the top end of the joint and served as the eyeball. Afterwards, some springs attached to electrically powered motors would pull the eyeball in a similar way as oculomotor muscles pull the eye.

The eye ball was designed as a semi sphere that would connect with the vanguard ball joint in the same way cameras are attached (see Figure 3.1). It´s diameter was to be as large as the 3D printing

machine allowed ($20 \times 15 \times 15\ cm$). There were two reasons for taking this size of the model. The first one was that the ball joint was big and had a total radius of $7\ cm$ which makes it impossible to make a semi sphere with a smaller radius than this and still have the centre of rotation in the centre of the joint. Subsequently, the drag forces would also be less in magnitude as we enlarged the sphere due the increasing torque when pulling the sphere.

Figure 3.1: Attachment of the semi sphere to the ball joint

The actuators were mounted accordingly with the muscles pulling directions. The final system is presented below in Figure 3.2:

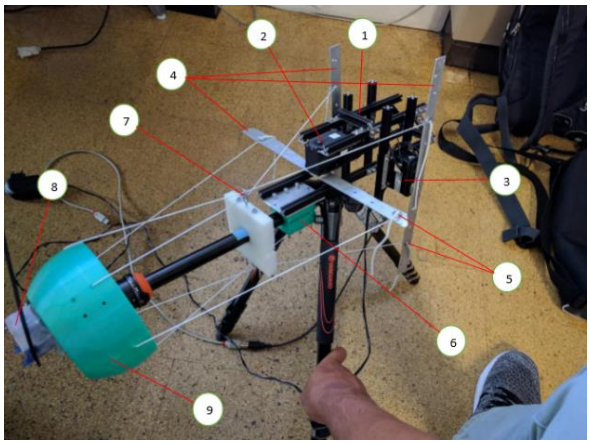

Figure 3.2: Assembled system. 1- Motor nº1 (IO & SO). 2- Motor nº2 (MR & LR). 3- Motor nº3 (SR & IR). 4- Motor aluminium arms. 5- Two out of six washers. 6- Compatibility part (3D printed adaptor). 7- Top modified eye screw. 8- LPMS-CU accelerometer sensor. 9- 3D printed eyeball

3.2. Software Architecture

More than one software package was used to control our model. Despite not being the simplest solution, it is the only possible one since some of the components that are being used such as the LPMS sensor, are not compatible with Linux. Furthermore, the embedded CM 900 board used to control the motors uses its own Arduino-like platform provided by RobotisTM.

Visual Studio 2015 was used to run the main C++ program. Boost libraries were installed so that communication via serial USB port with the motors became possible. The LPMS-CU libraries were also downloaded and compiled. The main C++ program sends and receives information via USB to the motors. Just after receiving data (position, velocity and force) from the motors, the program reads the position of the eyeball from the accelerometer, records it, and starts the loop yet again. Figure 3.3 shows a flow diagram of how the components are connected to each other.

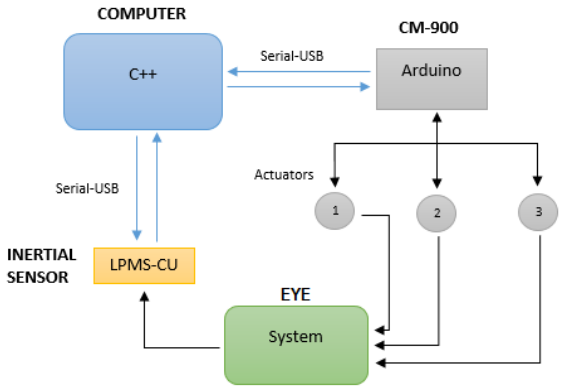

Figure 3.3: Flow diagram of the entire system+control

4. Results

4.1. Static System Identification

In order to identify our oculomotor system, we aimed to construct a mathematical model that would allow us to predict how the system would settle in its steady state for different inputs of the three motors. In other words, we should create a map of the 3D motor step inputs and the corresponding steady-state outputs (3D eye orientation), with the purpose of creating a function that could relate these variables.

The first test regarding this matter was done as follows. All three motors were moved to every possible position within their range from the initial starting position at straight ahead. As described before, this range was limited by the ball joint of the tripod, which cannot rotate more than $40°$, and it was also limited by the high muscle tensions which, as will be demonstrated, reduced the eye's orientation range to $\pm 30°$ with respect to straight ahead. We can tell, from Figure 4.1, that our system as it is, doesn't obey Donders' Law, and consequently, Listing's Law either. For an arbitrary 2D gaze direction (i.e., horizontal + vertical

component), our system can produce many torsional components. This means that our system, unlike the real eye, has in fact three position degrees of freedom for stationary fixations. Note that to specify an eye direction or gaze point, we only need two components, horizontal and vertical, and Donders' law holds that the torsional component should be uniquely fixed for each gaze direction.

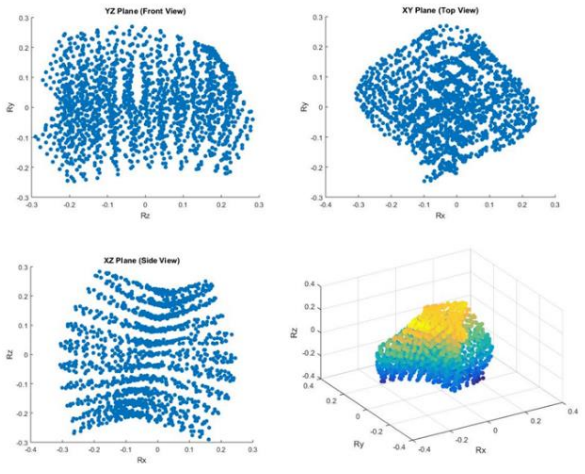

Figure 4.1: Oculomotor range within the YZ, XY, XZ plane and 3D expressed in rotation vectors notation. Units are in half-radians where 0.1 half-radians corresponds to about 10 degrees. R_z is a rotation around the z-axis, R_y is a rotation around the y-axis, and R_x is a rotation around the x-axis

To relate these rotation vectors to a particular plane, we parametrized a general plane by $R_x = d + bR_y + cR_z$. Where d represents the offset of the plane relative to the straight ahead configuration $(0,0,0)$, and R_x, R_y and R_z are the rotation vector components of all fixation points. We performed a brute force search through the parameter space of d, b, and c. To that end, the parameters were varied as follows $d = [-0.15, 0.15]$, $b = [-3.60, 3.60]$ and $c = [-3.60, 3.60]$, in order to produce 15059 different hypothetical planes. Afterwards, we set a maximum angular distance tolerated from a measured point to the plane created. The distance of a point (x_1, y_1, z_1) in rotation vector notation to a plane $(R_x + bR_y + cR_z + d = 0)$ is given by equation (4-1) (13):

$$Distance = \frac{|x_1 + by_1 + cz_1 + d|}{\sqrt{1^2 + b^2 + c^2}} \qquad (4\text{-}1)$$

This search was performed in Matlab. The program takes all the points from the data that we gathered, calculates their distance relative to the plane and stores the ones that meet the $3°$ distance criteria. This is done for all 15059 planes. We also attached to each plane characteristics the total amount of effort the motors had to produce to reach all the points englobed around the plane in question. This effort was normalized for each plane by taking into account the number of selected points, N, associated with that particular plane. It can range from 0 (minimum motor torque) to 1024 (maximum motor torque) and was calculated using equation (4-2).

$$E_{ff} = \frac{\sum \frac{e_{ff}}{3}}{N} \qquad (4\text{-}2)$$

where e_{ff} is a single motor effort corresponding to one measure of the N points. Each measure has three motor efforts associated, one for each of the three actuators.

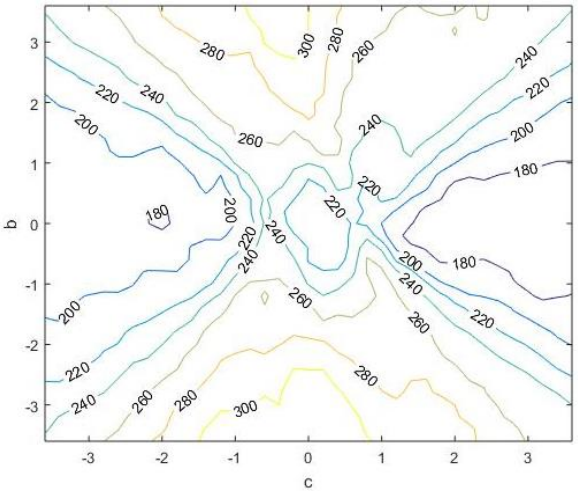

Figure 4.2: Contour plots of all planes where height is effort (E_{ff}). The traces represent the average effort for each plane defined by the coefficients b and c

In the contour plot of Figure 4.2 the absolute minima solutions seem to be a geometrical property of the model where the motor effort to keep the desired spatial orientation is minimized by applying loads of torsion. The plane $R_x = -2R_z$ doesn't even cover the entire oculomotor range since in Figure 4.1 we clearly see that the horizontal and torsional range is $\pm 30°$. We would have to be able to produce torsional rotations of up to $60°$ in order to have a gaze direction which horizontal component is $30°$ and that isn't possible. Nonetheless, there is another minimum, a relative minimum at position $(0,0)$. This means that the straight-ahead direction of our system could at the same time correspond to the primary position thus, already included in the $R_x = 0$, plane or in other words, Listing's plane. This could

actually make some sense because the straight ahead direction is the position for which our eye is at its resting position and the motor effort is at its minimum.

Figure 4.3 shows that the newly discovered plane ($R_x = 0$) has enough points (348 points) to cover a considerable range of $\pm 25°$ with respect to the straight-ahead position. In the side and top views we can see that the maximum displacement of the torsional component never exceeds our criteria of $3° \sim 0.03\ half\ radians$. It is also clear that these selected points respect both Donders' Law in good approximation (each gaze direction has one and only torsional component) and Listing's Law (the torsional component not only is a function of the vertical and horizontal components but also lie in a plane).

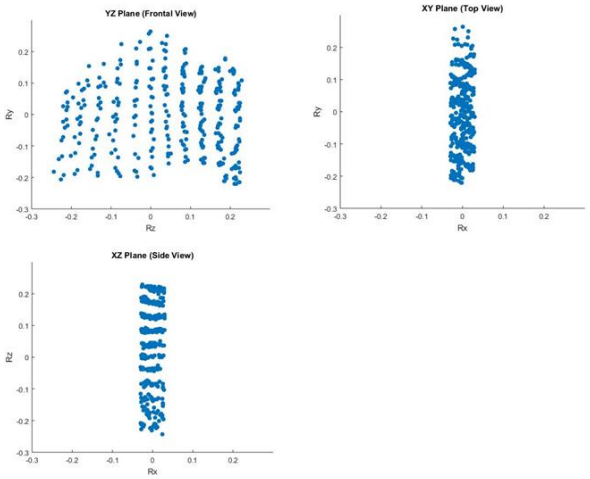

Figure 4.3: Frontal, top and side view of the plane $X = 0$. A 3° criteria was used to choose the points that satisfy the plane's condition. Units are in half-radians where 0.1 half-radians corresponds to about 10 degrees. R_z is a rotation around the z-axis, R_y is a rotation around the y-axis, and R_x is a rotation around the x-axis

During saccades, the eye orientations remain in the Listing's plane even though the high speed of the eye. Without any control four gaze directions forming a square were set and the eye moved from one to another clockwise (from the eye's point of view, +x). The result is shown in Figure 4.4 and, if all points were on Listing's plane, the outcome should be similar to Figure 2.3. Instead of following a straight line with $R_x = 0$ during the saccades, the torsional component deviates from this plane. This is more noticeable in the XZ plane. We will study in the next section the dynamics of our system and try to figure out what inputs should be given to produce saccades that comply with Listing's plane.

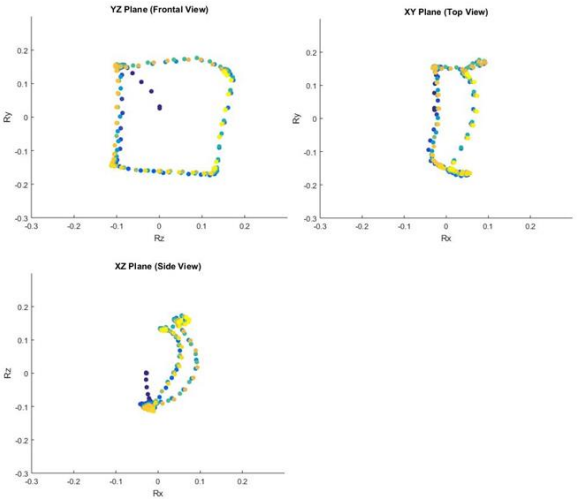

Figure 4.4: Recording of saccadic movements in a square alike shape around the primary position (0,0,0). Units are in half-radians where 0.1 half-radians corresponds to about 10 degrees. R_z is a rotation around the z-axis, R_y is a rotation around the y-axis, and R_x is a rotation around the x-axis

4.2. Dynamic System Identification

We here verify that our oculomotor model behaves as a nonlinear system. After some data analysis we noted that although it's a time invariant system, it doesn't obey the linearity (superposition) rules. In order for a system to be linear, it has to follow addition and homogeneity principles. A corollary from the superposition principle is that the movement durations of the eye should be independent of the step size. Figure 4.5 shows that this is clearly not the case. The movement duration, as we increase the amplitude for each saccade, instead of being constant, increases. The first indicator is that the peak velocity isn't doubling or tripling when the step input is doubled or tripled, which it should were the system to be linear. Note that the velocity never reaches the saturation point, as the threshold parameter was set to $680\ deg/s$. Also, the velocity peak, or maximum, should be growing vertically instead of shifting to the right. The actual problem is that the acceleration saturates meaning that for all four saccades, the motor's angular acceleration is at its maximum (at least at the beginning of the larger movements). This is confirmed because the velocity lines for 2s, 3s and 4s lie on top of each other, for example, yellow and purple are practically the same until just before the end when yellow is almost reaching the desired position.

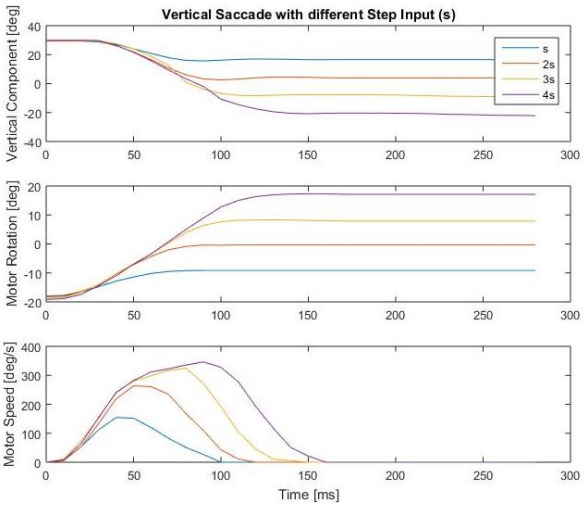

Figure 4.5: Eye orientation, motor position and speed of four Saccades where the amplitude of each step is multiple of s=9 degrees. Vertical component is pitch (ϕ)

Using Matlab's system identification tool, we determined the transfer functions for each of the four vertical saccades that were preformed to plot Figure 4.5. Interestingly, all four transfer functions resulted to be equal, which is in line with the hypothesis that this part of the System (eye + elastics) is Linear and Time Invariant. Additionally, the best fit is a second order system with one zero ($z_1 = -38.45$) and two poles ($p_1, p_2 = -68.85 \pm 5.72i$). The transfer function for vertical saccades obtained with Matlab explains 92% of the data, and is given in equation (4-3).

$$TF_v = \frac{\phi(s)}{\beta_v(s)} = \frac{-218s - 8382}{s^2 + 137.7s + 4773} \qquad (4\text{-}3)$$

where the static gain $K_{st} = -1.756$ and β_v is the vertical component input (SR & IO). In contrast to the real eye plant (see chapter 2), our model eye results to be slightly underdamped ($\zeta = 0.996$), which is caused by the complex poles. Note the negative signs in the nominator relate to the right-hand rule convention that upward movements are associated with negative angles.

Applying the same method as the one used to determine the vertical response system, a transfer function was obtained for pure horizontal and torsional movements. In this case, the angle β_h refers to the rotation of the single horizontal actuator (MR & LR) and β_t for SR&SO joint action:

$$TF_h = \frac{\theta(s)}{\beta_h(s)} = \frac{137.3s + 3527}{s^2 + 98.64s + 2091} \qquad (4\text{-}4)$$

$$TF_t = \frac{\psi(s)}{\beta_t(s)} = \frac{41.24s + 1807}{s^2 + 46.78s + 1059} \qquad (4\text{-}5)$$

From the three measurements in the cardinal directions, described above, it is not trivial to predict how the model will behave for oblique saccades into arbitrary gaze directions. In such movements, all three motors will be involved. So far, we've been simplifying the problem by removing two of either torsional, vertical or horizontal components. Recall that the inputs were parametrized from the initial three motor current positions to three motor combinations β_v, β_h and β_t, and the output is the eye's spatial orientation defined by Euler angles (ZYX). As for the whole system, it means that we have only calculated the diagonal (G_{11}, G_{22}, G_{33}) of the 3×3 transfer function matrix.

Due to the complexity of characterizing all the entries of the matrix, we thus assume that the system is not coupled. This means that an actuator's torsion input β_t for example, will not produce nor influence vertical and horizontal rotations. The same would happen for vertical β_v or horizontal β_h inputs and therefore, all off-diagonal elements ($G_{12}, G_{13}, G_{23}, G_{21}, G_{31}, G_{31}$) are assumed to be zero. To verify if this approximation may apply to our system, we performed a couple of oblique saccades.

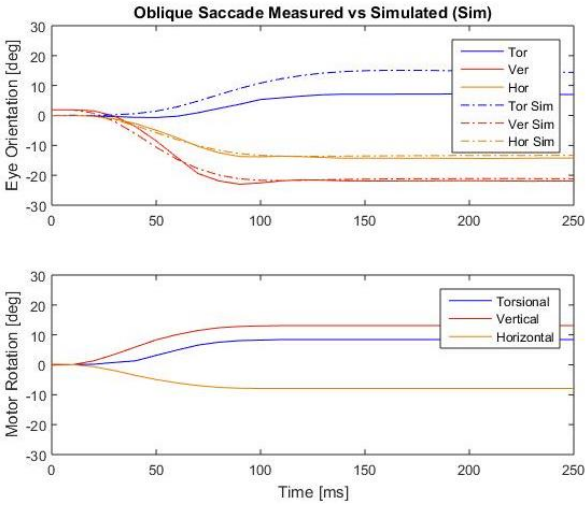

Figure 4.6: Comparison of the Torsional (Tor), vertical (Ver) and Horizontal (Hor) components of an oblique saccade with a simulation (Sim). The motor rotation is the input. Vertical component is pitch (ϕ), horizontal component is yaw (θ) and torsional component is roll (ψ)

From Figure 4.6 we may infer that for this example the model is able to predict the vertical and the horizontal components of an oblique saccade,

because in both cases, the measured line (full) and the simulated line (dash-dotted) are practically superimposed. It means that for our system, the vertical and the horizontal degrees of freedom have little interaction between them and may be considered to be decoupled from each other. On the other hand, the same cannot be said for the torsional component. The simulated response is faster (reacting) and larger than the real measured response, and even the steady state isn't the same. This happens because the vertical and horizontal components both have an effect on torsion.

Up to now, we characterized the dynamics of the linear part of our system (elastics + eye). The full system, from computer-command step input to eye-movement output, should also include the actuator's dynamics. Unfortunately Robotis doesn't provide the Dynamixel's internal control and transfer functions. Nevertheless, we know how a typical DC motor is constructed and thus, we built an approximation model for the actuators, depicted below in Figure 4.7. We used this model to make simulations and compare them to the actual motor's response so that the control and physical parameters were estimated and made approximately the same.

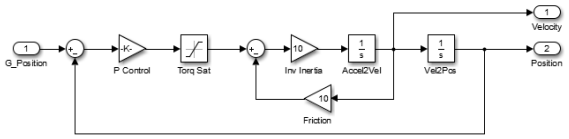

Figure 4.7: Simulink of the approximation model of the actuator

5. Conclusions

With the characterization of the non-linear part of the plant (motors), we are now able to determine exact inputs that will provide the response that most resembles a human saccade. It is almost guaranteed that these inputs will not be compatible to our motors since their control variables are very limited. Nevertheless, this will provide us some requirements where we could base ourselves in order to buy actuators that better meet the required specifications (i.e. velocity control, acceleration control).

This first prototype was based on low cost and overall implementation simplicity. Yet, this approach already provided us with novel insights into the real control of such a system. For example, the effects of cable tension and motor position were rather difficult to predict a priori, let alone the behaviour of the system to determine Listing's plane for our system.

6. Bibliography

1. **Bernstein, Nikolai.** *The Coordination and Regulation of Movements.* Oxford : Pergamon Press, 1967.

2. **Saladin, Kenneth S.** *Anatomy & physiology: the unity of form and function.* New York : McGraw-Hill, 2012. ISBN 978-0-07-337825-1.

3. **Carpenter, Roger H.S.** *Movements of the eyes.* London : Pion, 1988.

4. **TeachMeAnatomy.** TeachMeAnatomy. *http://teachmeanatomy.info/head/organs/eye/extraocular-muscles/.* [Online] [Cited: 08 08 2017.]

5. **Opstal, John Van.** *Three-Dimensional Kinematics Underlying Gaze Control.* Medical Physics and Biophysics, University of Nijmegen. Nijmegen, The Netherlands : Springer Verlag, 1998.

6. —. *Representation of eye position in three dimensions.* University of Nijmegen. Nijmegen, The Netherlands : s.n., 1993.

7. **Donders, F. C.** *On the Anomalies of Accomodation and Refraction of the Eye.* London : New Sydenham Society, 1864.

8. **Liversedge, Simon, Gilchrist, Lain and Everling, Stefan.** *The Oxford Handbook of Eye Movements.* Oxford : Oxford University Press, 2011. ISBN 978-0-19-162661-6.

9. **Cromer, J.A. and Waitzman, D.M.** *Neurones associated with saccade metrics in the monkey central mesencephalic reticular formation.* s.l. : J Physiol, 2006. 570.3:507-523.

10. **Kandel, E.R., Schwartz, J.H. and Jessell, T.M.** *Principles of Neural Science* . s.l. : McGraw-Hill (4th ed.), 2000. ISBN 0-07-112000-9.

11. **Opstal, John van.** *The Auditory System and Human Sound-Localization Behavior.* London, UK : Elsevier, 2016. ISBN: 978-0-12-801529-2.

12. **Robinson, David A.** *Models of the saccadic eye movement control system.* s.l. : Biologic Cybernetics, 1973. Vol. 14.

13. **Opstal, John Van.** *Two- Rather Than Three-Dimensional Representation of Saccades in Monkey Superior Colliculus.* s.l. : Science, 1991.